Mechanisms in iron, nickel, and manganese, catalysis with small molecule oxidants

Padamati, Sandeep K.

Chapter 3
Solvent switching of the selectivity of a Non-Heme Fe(II) complex in the oxidation of alkenes

Abstract

The complex [(MeN3Py)$Fe^{II}(CH_3CN)_2](ClO_4)_2$ (**1**), has been shown to catalyze the oxidation of alkenes with H_2O_2 to 1,2-diols, as well as epoxides. The oxidation of *cis*-cyclooctene with H_2O_2 leads to its *cis*-diol product in acetonitrile, but was reported to yield the *trans*-diol product in acetone. In this chapter we show that **1** forms a transient Fe(III)-OOH species upon reaction with H_2O_2, which undergoes homolysis to form an Fe(IV)=O species and, ultimately, a thermodynamically stable Fe(III)-O-Fe(III) acetato bridged dimer. The reaction of the Fe(IV)=O species with *cis*-cyclooctene is demonstrated to form cyclooctene epoxide. In the presence of acetic acid the rate of formation of both the Fe(IV)=O species and the Fe(III)-O-Fe(III) acetato dimer is accelerated. Furthermore, we show that the Fe(III)-OOH species formed upon reaction of **1** with H_2O_2 is stable at low temperatures (193 K), enabling its characterization by UV-vis absorption, EPR and ESI-mass spectroscopy.

Sandeep K. Padamati, Duenpen Unjaroen, Laura Gomez, Anna Company, Wesley R. Browne, to be submitted

3.1 Introduction

The catalytic oxidation of hydrocarbons using economically and environmentally friendly oxidants, in particular H_2O_2, is of substantial importance.[1,2,3] The development of such catalytic systems faces many challenges, in particular with regard to selectivity and efficiency under ambient conditions. Nature engages oxidation catalysis using enzymes, to carry out a wide range of C-H oxidation reactions, for example arenes are oxidized to alcohols by oxidases such as Rieseke dioxygenase.[4] In the catalytic site in napthalene dioxygenase, which oxidises napthelene to napthelene diol, two histidines and a bidentate aspartic acid coordinate to an Fe(II) ion, leaving two exchangeable sites for the coordination of water and oxidant.[4] Synthetic systems inspired by these enzymes have focused heavily on non heme iron polypyridyl complexes,[5] and indeed these classes of complexes are catalytically active in the epoxidation and *cis*-dihydroxylation of alkenes, as well as oxidation of alkyl C-H bonds to alcohols and ketones, using H_2O_2 as terminal oxidant.[6] Feringa and coworkers have shown that complexes of N4 donor ligands, specifically $[(MeN3Py)Fe(II)(CH_3CN)_2](ClO_4)_2$ (**1**) are active in alkene dihydroxylation and epoxidation. The complex $[(MeN3Py)Fe(II)(CH_3CN)_2](ClO_4)_2$ (**1**), can catalyze the oxidation of alkenes to 1,2-diols, as well as epoxides. The oxidation of *cis*-cyclooctene with H_2O_2 and **1** was reported to lead to its *cis*-diol product in acetonitrile, however, the *trans*-diol product was observed in acetone.[7] This effect of solvent on the selectivity of catalyst was rationalized by the differences in the stability of Fe(III)-OOH and Fe(IV)=O intermediates that were proposed to form under reaction conditions. In acetone, the CH_3CN ligands of **1** were proposed to exchange with water present in the solvent, and addition of H_2O_2 leads to the formation of an Fe(III)-$OO(CH_3)_2COH$ species. Subsequently, homolysis would form an Fe(IV)=O species and the radical $\bullet O(CH_3)_2COH$, which then reacts with alkenes to form the trans product. Recent studies by Que,[8] Akimova[9] and co-workers indicate that Fe(III)-OOH species do not engage directly in the oxidation of alkenes and C-H oxidation, instead high valent Fe(IV)=O and Fe(V)=O species formed by O-O bond homolysis and heterolysis are proposed to react with substrates.[10,11] Furthermore, it is apparent that the site on the metal complex, in N4 ligated systems, that can exchange with solvent, plays a crucial role in determining selectivity and in stabilizing high valent iron species. Hence, gaining insight into these systems and the role of solvent as a ligand is central to controlling selectivity and reactivity.

In Chapter 2, the formation of an Fe(III)-OOH species upon reaction of complex $[(MeN3Py)Fe(II)(CH_3CN)]^{2+}$ (**1**) with H_2O_2 at room temperature is discussed. Formation of the Fe(III)-OOH species, and its subsequent conversion to relatively inert Fe(III)-O-Fe(III) species, was shown to be highly sensitive to the presence of water, with excess water favoring formation of the kinetically inert dinuclear species (with respect to ligand exchange). The addition of acetic acid increased the rate and extent of oxidation of **1** to its ferric state but did not affect significantly the spectroscopic properties of the Fe(III)-OOH species formed.

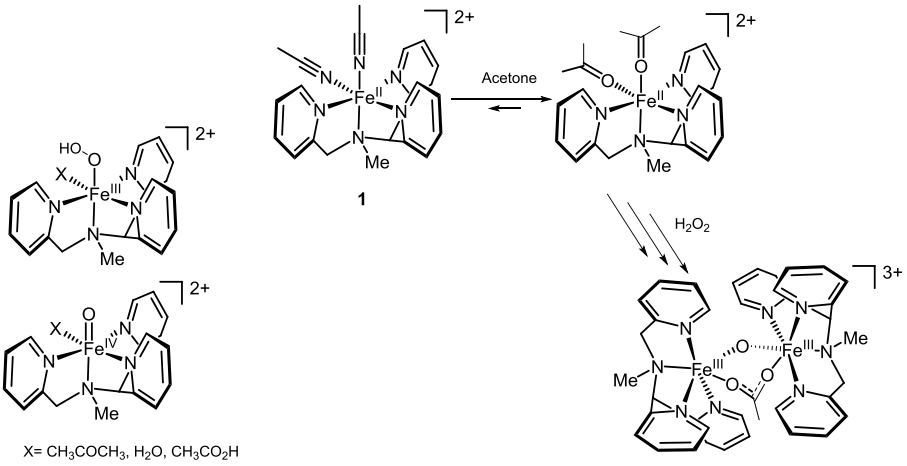

Scheme 1 Reactions of **1** with H_2O_2 in acetone and structures of species discussed in the text

In this chapter, we provide spectroscopic evidence for the formation of an Fe(III)-OOH and subsequently an Fe(IV)=O species upon reaction of **1** with H_2O_2 in acetone at room temperature. The decay of these species to a thermodynamically stable Fe(III)-O-Fe(III) acetato bridged dimer is shown to occur in acetone, due to *in situ* generation of acetic acid, and furthermore, formation of Fe(III)-O-Fe(III) acetato bridged dimer is accelerated by addition of acetic acid to reaction mixture. The Fe(IV)=O species formed is shown to react rapidly with *cis*-cyclooctene to form cyclooctene epoxide.

3.2 Results

The synthesis and X-ray structural characterization of $[(MeN3Py)Fe(II)(CH_3CN)_2](ClO_4)_2$ (**1**) was described earlier (chapter 2).[12] The ^1H NMR spectrum of **1** in CD_3COCD_3 (Figure 1) shows signals in the range 0 - 170 ppm, indicative of a paramagnetic high spin iron(II) complex,[7,12,13] in which the CH_3CN ligands of **1** have exchanged with CD_3COCD_3 (or adventitious water), to form the high spin complex $[(MeN3Py)Fe^{II}(S)_2]^{2+}$ (where S = CD_3COCD_3 or H_2O).

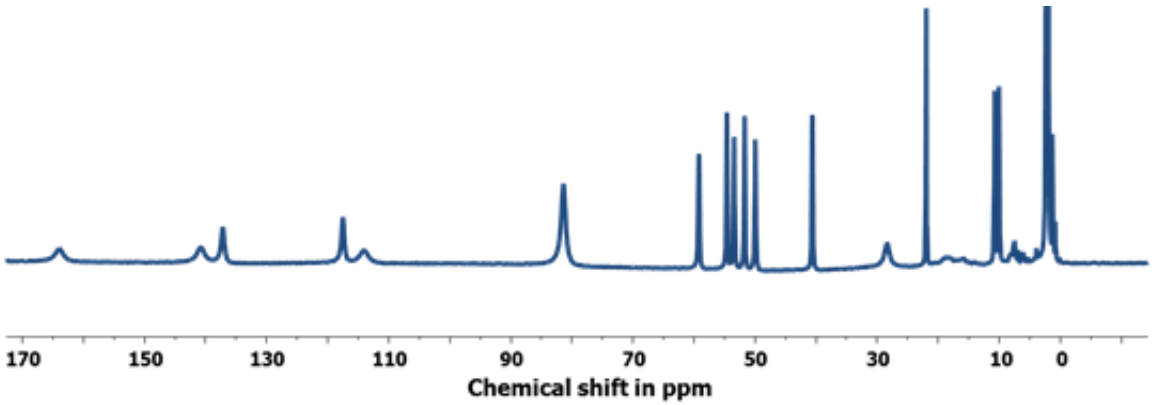

Figure 1 ^1H NMR 400 MHz spectrum of **1** (12.5 mM) in CD_3COCD_3.

The change is consistent with the decrease (70%) in the molar absorptivity and blue shift of the visible absorption bands (Figure 2), and shift in redox potential compared with that of **1** in CH_3CN (vide infra). Notably, the UV-vis absorption spectrum of **1** in water is not similar to that in acetone, consistent with coordination of acetone.

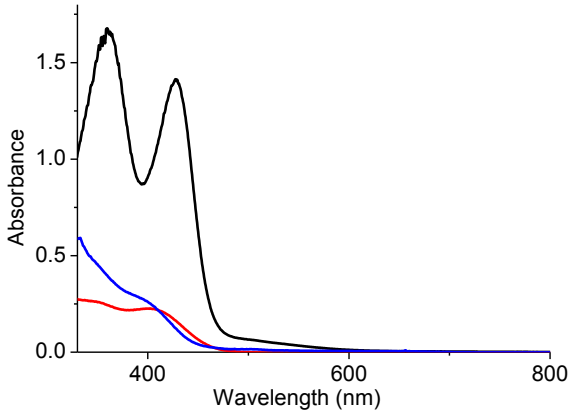

Figure 2 UV-vis absorption spectrum of **1** (0.25 mM) in acetone (blue), acetonitrile (black), and water (red).

There is a substantial increase in the visible absorption bands upon addition of > 0.1 M CH_3CN. Addition of CH_3CN up to 1.4 M, resulted in 50% of recovery in visible absorption (Figure 3, green) with a spectrum similar to that observed for **1** in CH_3CN (Figure 3, blue).

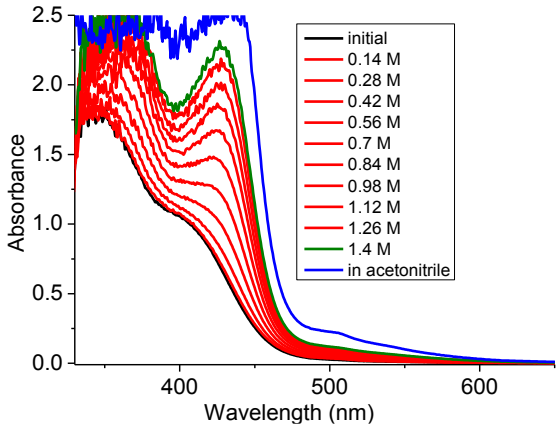

Figure 3 UV-vis absorption spectra of **1** (1 mM) in acetone (black) and with added CH_3CN (0.14 to 1.40 M, red), and **1** (1 mM) in acetonitrile (blue). Spectra are corrected for dilution.

The cyclic voltammogram of **1** in acetone shows a chemically irreversible oxidation ($Fe^{III}/Fe^{II}((CH_3)_2CO)_2$) at $E_{p,a}$ 0.95 V, and subsequent reductions at 0.79 V, and 0.34 V vs. SCE (Figure 4). The redox wave at 0.34 V is assigned, tentatively, to the $Fe^{III}/Fe^{II}(OH_2)((CH_3)_2CO)$ redox couple. Increasing the scan rate from 0.1 to 10.0 V s^{-1} resulted in the shift of $E_{p,a}$ from 0.95 to 1.07 V, and the increase in a redox wave at 0.65 V on the return cycle, and a disappearance of redox wave at $E_{p,c}$ 0.34 V, replaced by an additional redox wave at 0.11 V (Figure 4).

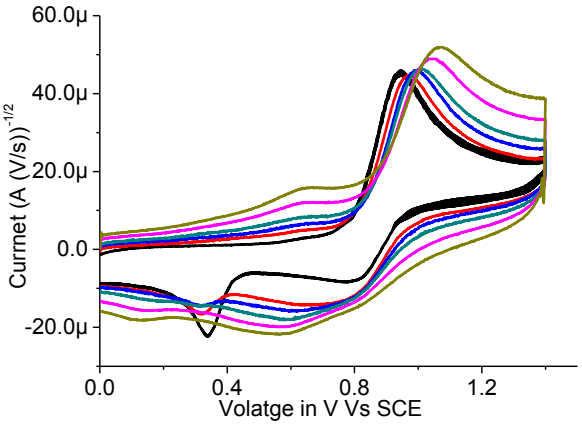

Figure 4 Cyclic voltammetry of **1** (1mM) in acetone (0.1 M $TBAPF_6$) with increase in scan rate from 0.1 (black), 0.5 (red), 1.0 (blue). 2.0 (green), 5.0 (pink), 10.0 (olive green) V s^{-1}. Current is divided by $\sqrt{scan\ rate}$.

3.2.1 Reaction of 1 with H_2O_2 in acetone

The reaction of **1** with near stoichiometric amounts of H_2O_2 (1 to 10 eq.) in acetone was studied in the absence and presence of acetic acid.

UV-vis absorption spectroscopy at room temperature

With 1 equiv. H_2O_2, a rapid decrease in visible absorbance, and a concomitant increase in absorbance at ca. 503 and 755 nm[10] (the latter assigned tentatively to an Fe(IV)=O species) was observed, followed by a decrease in the NIR absorption (Fe(IV)=O species) and concomitant increase in absorbance at 457, 500, 539, and 690 nm. Notably, the NIR absorbance is shifted by 30 nm to longer wavelengths (from 725 nm to 755 nm) compared to that observed in acetonitrile (chapter 3). The final absorption spectrum is characteristic of Fe(III)-O-Fe(III) acetato bridged dimer (Figure 5).[12]

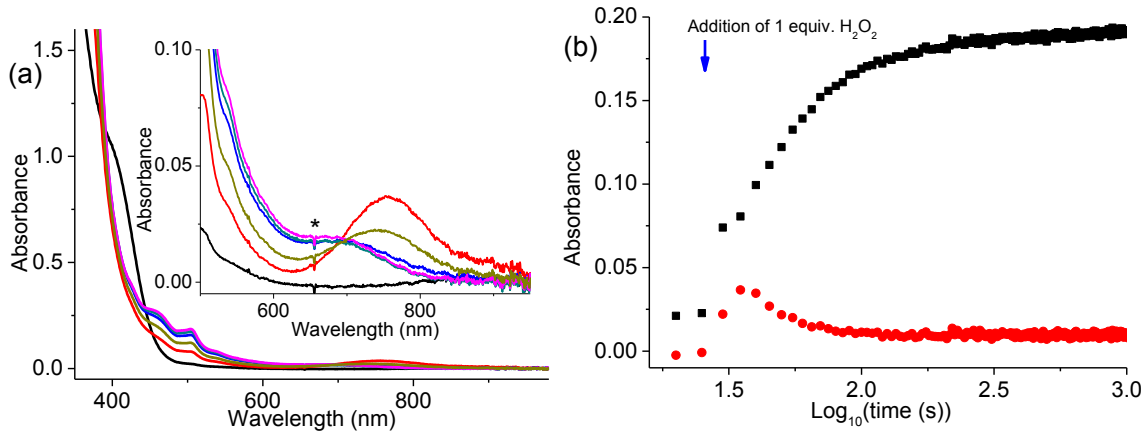

Figure 5 UV-vis absorption spectrum of **1** (1 mM) in (a) acetone (black) before, and after addition of 1 equiv. H_2O_2, 5 s (red), 20 s (grey), 50 s (blue), 100 s (green), and 300 s (pink), and (b) time dependence of absorbance at 503 nm (black) and 755 nm (red). Inset: expansion from 500 - 950 nm. * Instrumental artefact.

Similarly, with 2, 5 or 10 equiv. H_2O_2 the visible absorbance of the Fe(II) complex (at 410 nm) decreases rapidly concomitant with an increase in absorbance at 755 nm, and ultimately formation of an Fe(III)-O-Fe(III) acetato bridged dimer was observed (Figures 6 - 8). Notably, the maximum absorbance at 755 nm (giving an estimated 25% conversion of **1** to Fe(IV)=O based on a molar absorptivity[14] of 300 M^{-1} cm^{-1}) is reached with 5 equiv. H_2O_2, and the maximum reached is lower with 10 equiv. H_2O_2 (Figure 8). Furthermore, an isosbestic point is not maintained between the 503 and 785 nm absorption bands with 5 and 10 equiv. indicating the involvement of a second pathway, such as reaction of Fe(IV)=O with H_2O_2 (vide infra) and that the acetato bridged Fe(III)-O-Fe(III) dimer is not formed directly upon Fe(IV)=O reduction.

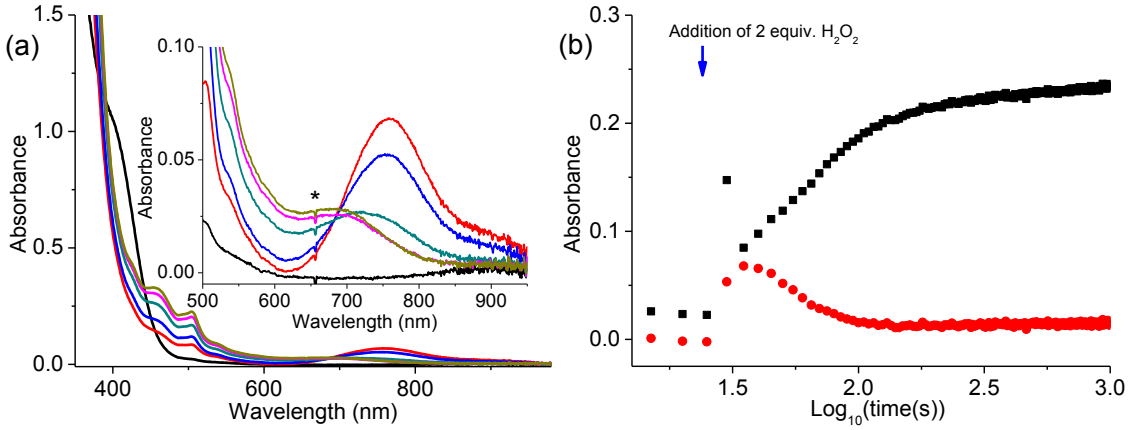

Figure 6 UV-vis absorption spectrum of **1** (1 mM) in (a) acetone (black) before, and after addition of 2 equiv. H_2O_2 4 s (red), 20 s (blue), 50 s (green), 100 s (pink), and 300 s (grey), and (b) time dependence of absorbance at 503 nm (black) and 755 nm (red). Inset: expansion from 500 - 950 nm. * Instrumental artefact.

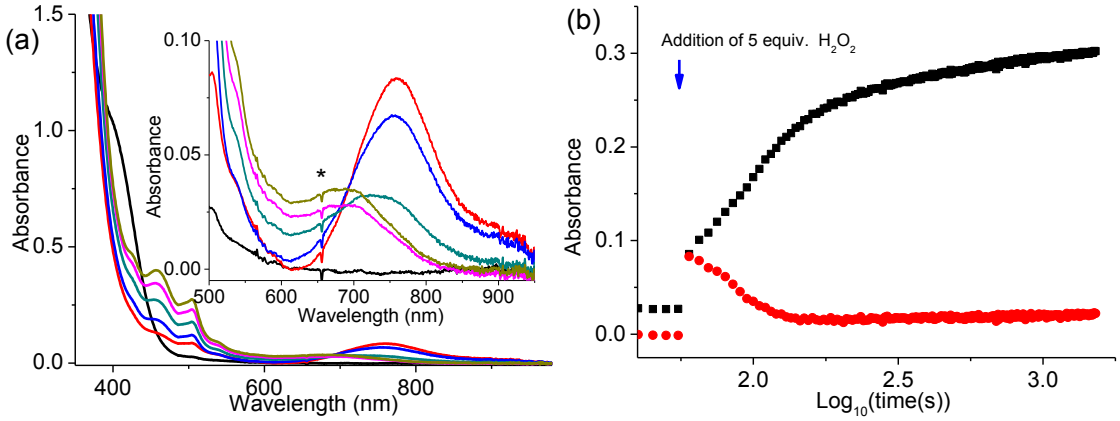

Figure 7 UV-vis absorption spectrum of **1** (1 mM) in (a) acetone (black) before, and after addition of 5 equiv. H_2O_2 5 s (red), 20 s (blue), 50 s (green), 100 s (pink), and 300 s (grey), and (b) time dependence of absorbance at 503 nm (black) and 755 nm (red). Inset: expansion from 500 - 950 nm. * Instrumental artefact.

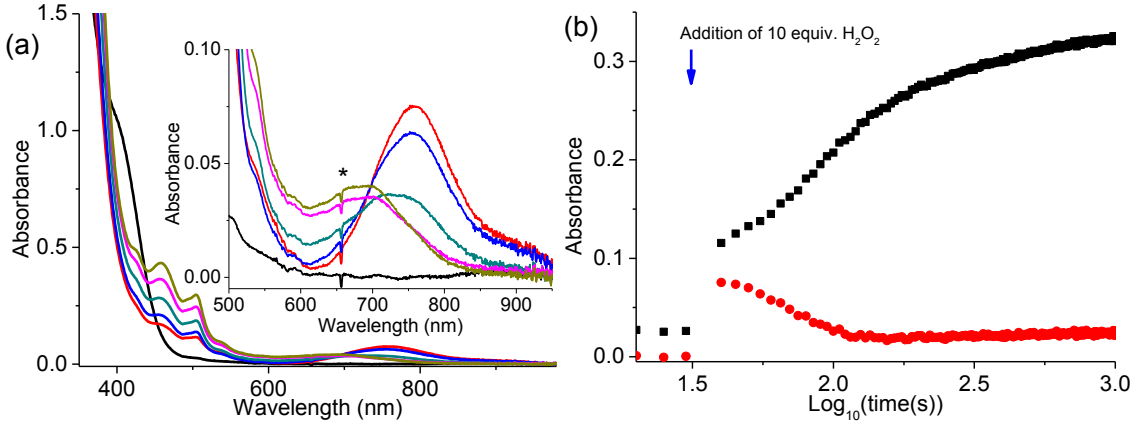

Figure 8 UV-vis absorption spectrum of **1** (1 mM) in (a) acetone (black) before, and after addition of 10 equiv. H_2O_2 5 s (red), 20 s (blue), 50 s (green), 100 s (pink), and 300 s (grey), and (b) time dependence of absorbance at 503 nm (black) and 755 nm (red). Inset: expansion from 500 - 950 nm. * Instrumental artefact.

Addition of 25 or 100 equiv. H_2O_2 to **1** resulted in an immediate increase in broad absorbance at 503 nm tentatively assigned to Fe(III)-OOH species with a concomitant increase in the NIR absorbance due to the Fe(IV)=O species (Figure 9 and Figure 10). Subsequently, both absorption bands decrease with appearance of the characteristic absorption spectrum of the Fe(III)-O-Fe(III) acetato dimer. It should be noted that the maximum absorbance at 755 nm with 100 equiv. H_2O_2 (Figure 10) is significantly lower than that with 10 equiv. H_2O_2 (vide supra).

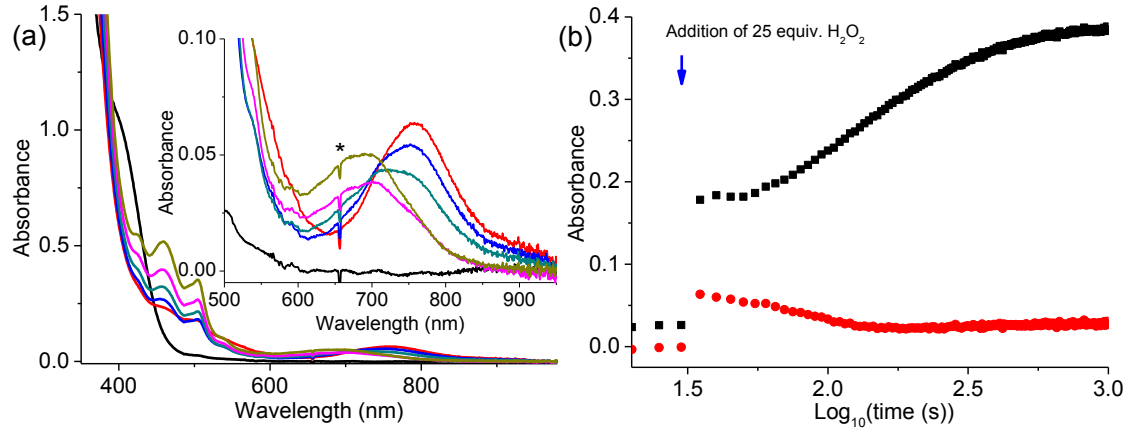

Figure 9 UV-vis absorption spectrum of **1** (1 mM) in (a) acetone (black) before, and after addition of 25 equiv. H_2O_2 5 s (red), 20 s (blue), 50 s (green), 100 s (pink), and 300 s (grey), and (b) time dependence of absorbance at 503 nm (black) and755 nm (red). Inset: expansion from 500 - 950 nm. * Instrumental artefact.

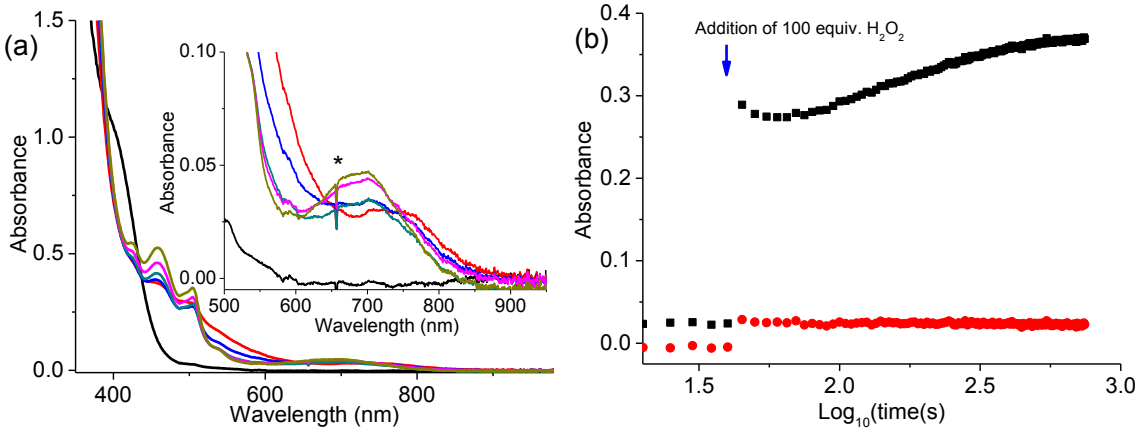

Figure 10 UV-vis absorption spectrum of **1** (1 mM) in (a) acetone (black) before, and after addition of 100 equiv. H_2O_2 5 s (red), 20 s (blue), 50 s (green), 100 s (pink), and 300 s (grey), and (b) time dependence of absorbance at 503 nm (black) and755 nm (red). Inset: expansion from 500 - 950 nm. * Instrumental artefact.

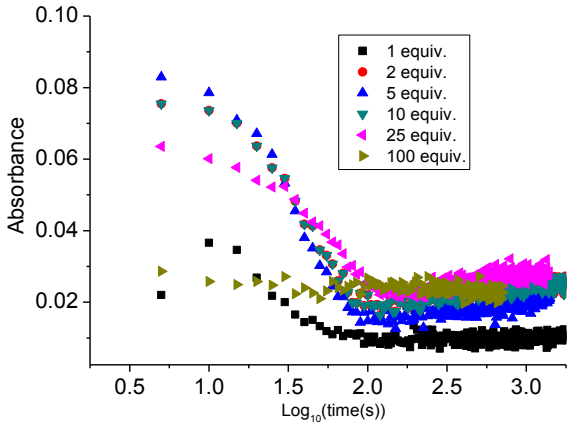

Figure 11 Time dependence of absorbance at 755 nm upon addition of 1 - 100 equiv. of H_2O_2 to **1** (1 mM) in acetone at room temperature.

Cyclic voltammetry at room temperature

The cyclic voltammogram of **1** changes dramatically after addition of 1 equiv. H_2O_2 with a 90% decrease in the $I_{p,a}$ of the $Fe^{III}/Fe^{II}(CH_3CN)$ redox couple (Figure 12) in agreement with changes observed by UV-vis absorption spectroscopy (Figure 5). Notably, the redox wave at ca. $I_{p,c}$ 0.35 V on the return cycle decreases with the appearance of an irreversible redox wave at 0.09 V consistent with the formation of an Fe(III)-O-Fe(III) dimer (vide supra).[12]

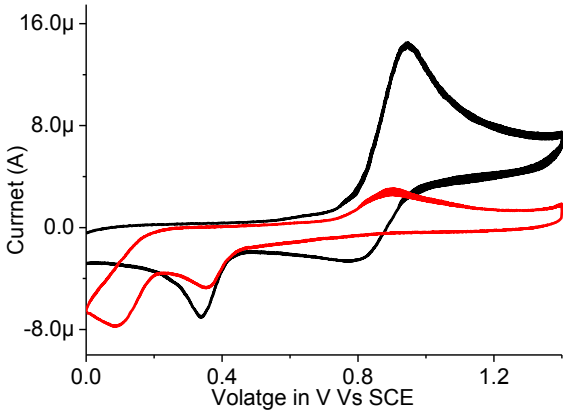

Figure 12 Cyclic voltammetry of **1** (1 mM) in acetone (0.1 M $TBAPF_6$) before (black) and after (red) addition of 1 equiv. H_2O_2 (red). Scan rate 0.1 V s^{-1}.

^{1}H NMR spectroscopy at room temperature

Addition of 10 equiv. H_2O_2 to **1** in CD_3COCD_3 results in a shift of signals in the ^{1}H NMR spectrum up-field to yield a spectrum consistent with the formation of an antiferromagnetically coupled Fe(III)-O-Fe(III) acetato dimer (Figure 13).[12]

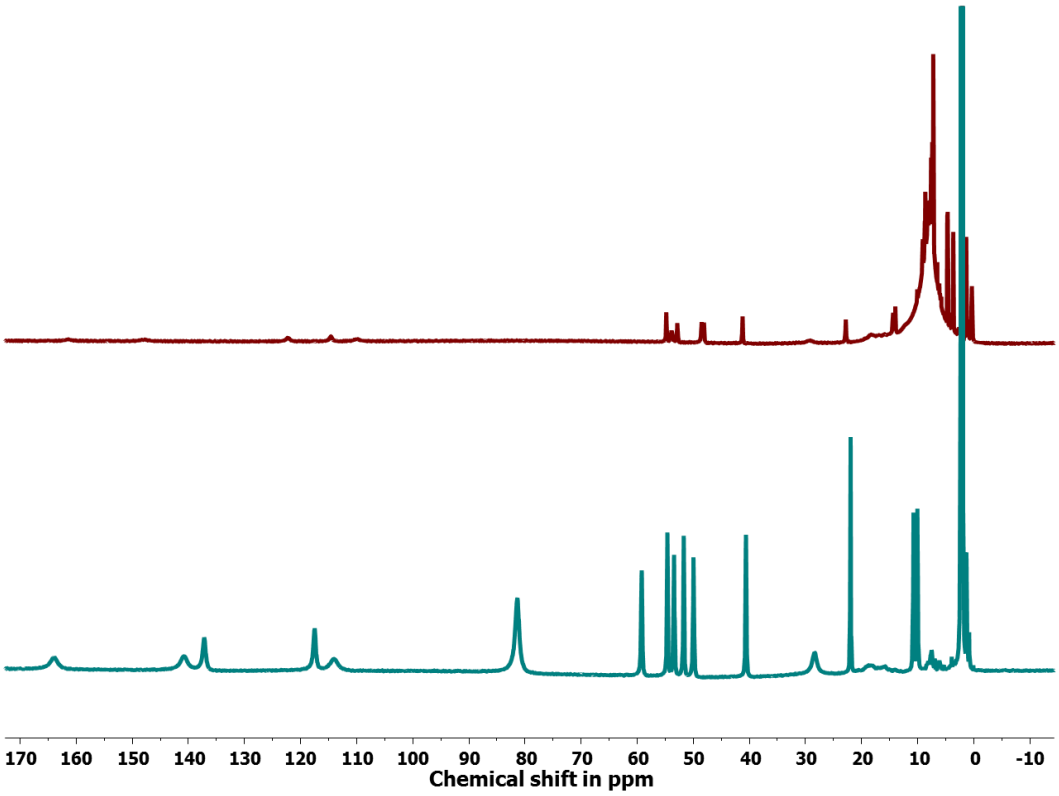

Figure 13 ^{1}H NMR spectra of **1** (12.5 mM) in CD_3COCD_3 (blue), and after addition of 10 equiv. H_2O_2 to 1 (14 mM) in CD_3COCD_3 (red). All spectra recorded at 400 MHz.

UV-vis absorption spectroscopy at -30 °C

Addition of 1 equiv. H_2O_2 to **1** in acetone resulted in an immediate decrease in absorbance at 400 nm, with a concomitant increase in absorbance at 503 nm (ascribed to an Fe(III)-OOH species). The absorbance at 503 nm subsequently decreases with the absorbance at 755 nm (ascribed to an Fe(IV)=O species) continuing to increase. The NIR absorbance of the Fe(IV)=O species decays more slowly (over ca. 400 s) than at 20 °C (Figure 14a). Addition of 5 equiv. H_2O_2 results in similar changes with only a marginal increase in the maximum absorbance at 503 nm reached (Figure 14c).

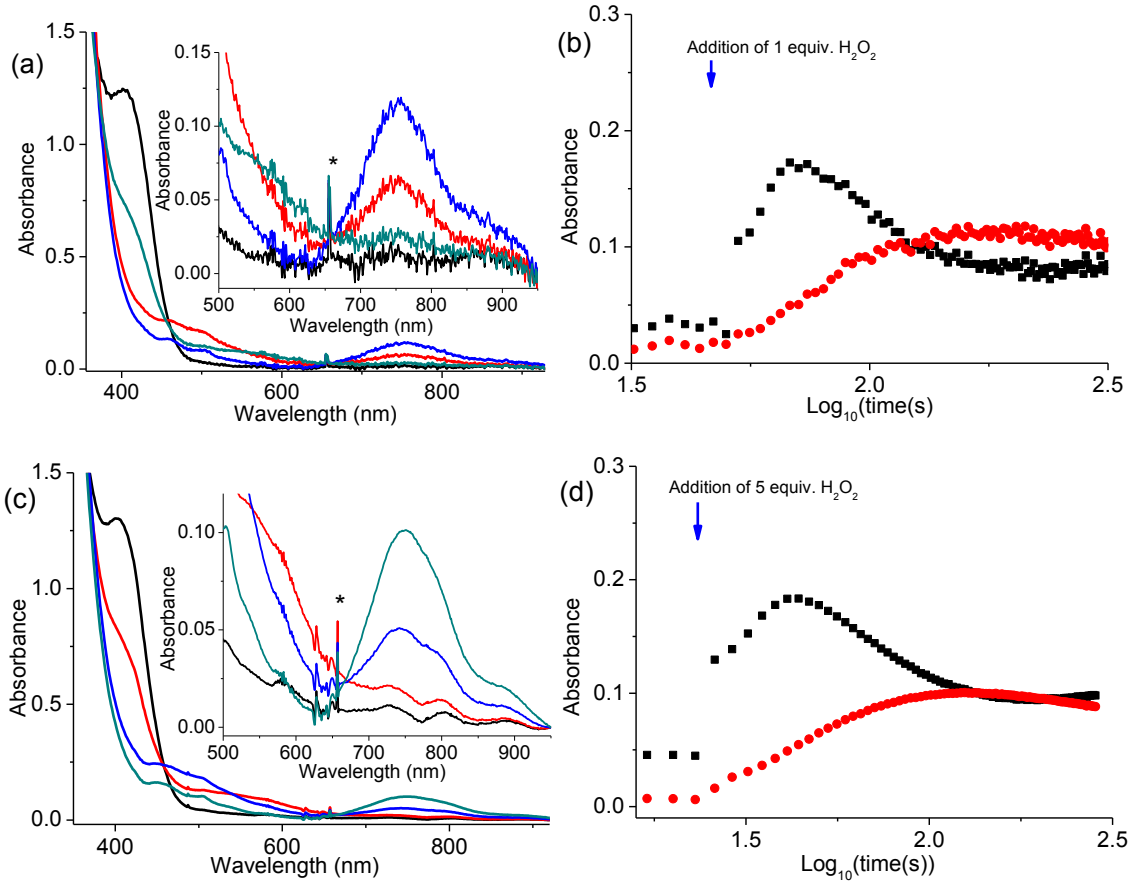

Figure 14 UV-vis absorption spectrum of 1 (1 mM) in acetone (black) at -30 ºC before, and (a) after addition of 1 equiv. H_2O_2 , 4 s (green), 24 s (red), and 123 s (blue), (c) after addition of 5 equiv. H_2O_2, 3 s (red), 18 s (blue), and 100 s (green). (b) and (d) corresponding time dependence of absorbance at 503 nm (black) and 755 nm (red). Inset: expansion from 500 - 950 nm. * Instrumental artefact.

With 10 equiv. H_2O_2 the maximum initial absorbance reached at 503 nm is substantially greater than with 1 or 5 equiv. H_2O_2, however, the maximum extent of formation of the Fe(IV)=O species (i.e. the NIR absorbance) is less (Figure 15). With 25 or 100 equiv. H_2O_2 the spectral changes were substantially different. Again, the absorbance at 503 nm increased concomitant with a decrease in absorbance at 400 nm with a further increase in the maximum absorbance reached at 503 nm to 0.4 and 0.5, respectively (Figure 16).

Furthermore, whereas the decay of the Fe(III)-OOH species begins immediately after its absorbance maximizes in the case of 25 equiv. H_2O_2, with 100 eq. the maximum absorbance is maintained for a substantial period of time prior to the onset of its decay, indicating that it is regenerated continuously until all H_2O_2 is consumed. Notably, the extent of formation of the NIR absorption band of the Fe(IV)=O species was reduced with increased equiv. of H_2O_2 and in all cases the appearance of the characteristic absorption spectrum of the Fe(III)-O-Fe(III) acetato bridged dimer is delayed (by 300s) compared to room temperature.

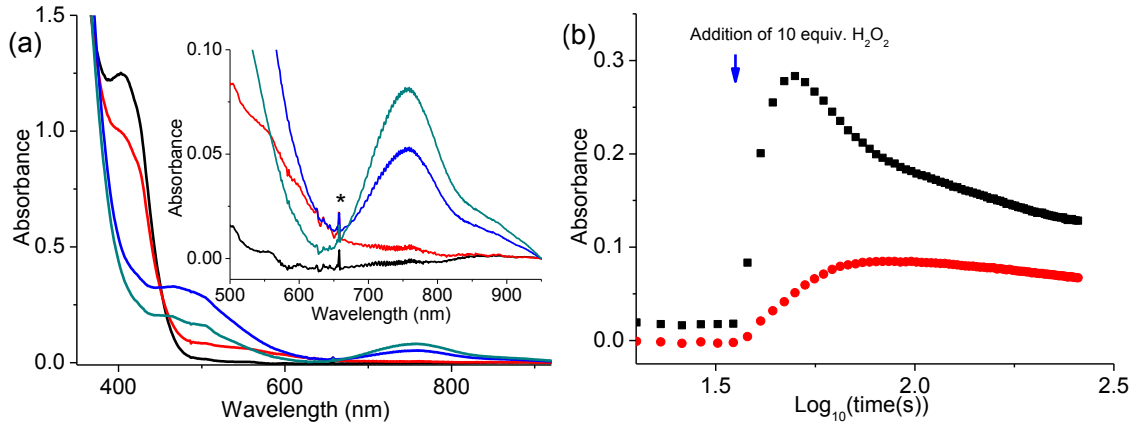

Figure 15 UV-vis absorption spectrum of **1** (1 mM) in acetone (black) at -30 ºC before, and (a) after addition of 10 equiv. H_2O_2, 3 s (red), 15 s (blue), and 100 s (green), and (b) time dependence of absorbance at 503 nm (black) and 755 nm (red). Inset: expansion from 500 - 950 nm. * Instrumental artefact.

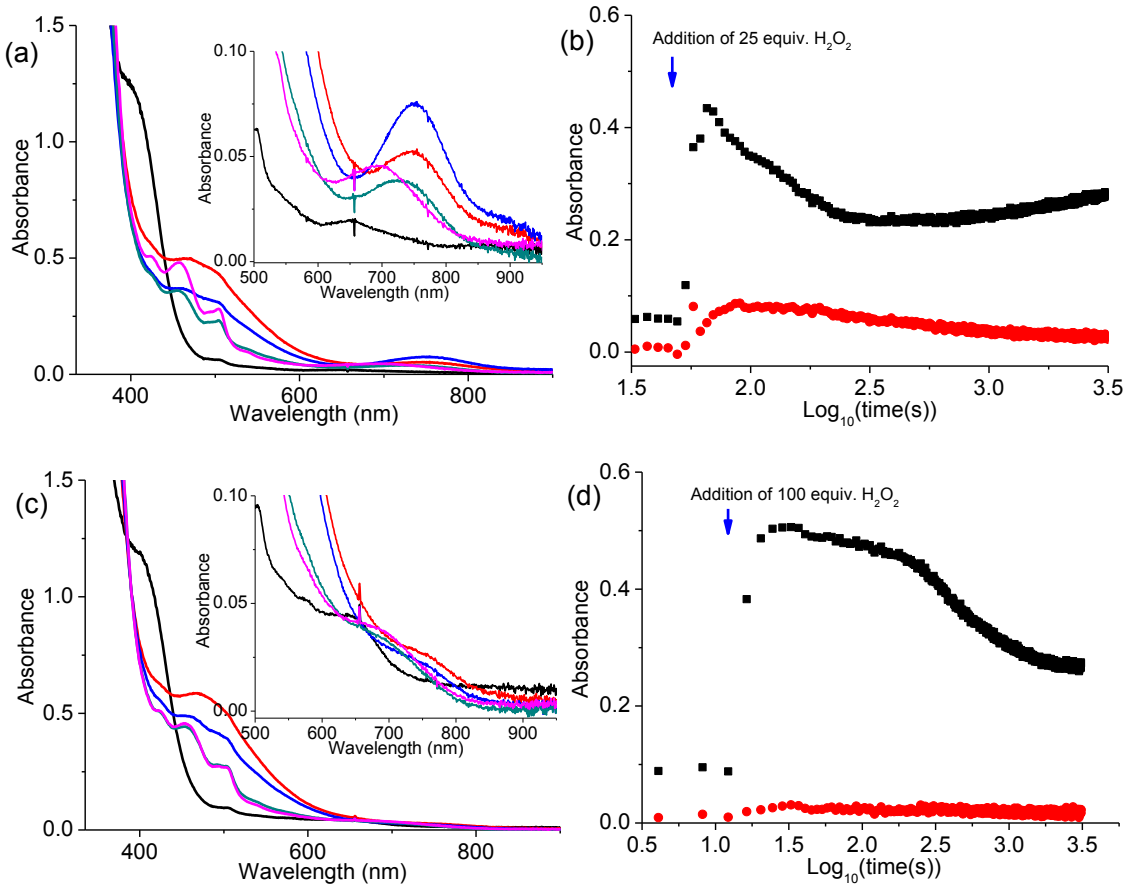

Figure 16 UV-vis absorption spectrum of **1** (1 mM) in acetone (black) at -30 ºC before, and (a) after addition of 25 equiv. H_2O_2, 8 s (red), 80 s (blue), 673 s (green) and 2928 s (pink), (c) after addition of 100 equiv. H_2O_2, 8 s (red), 354 s (blue), 1988 s (green) and 2972 s (pink), (b) and (d) corresponding time dependence of absorbance at 503 nm (black) and 755 nm (red).

UV-vis absorption spectroscopy at -80 ºC

At -80 ºC the visible absorbance of **1** was substantially greater than at room temperature, indicative of an increase in the proportion of the complex in the low spin Fe(II) state (vide infra). Addition of 1 equiv. H_2O_2 to **1** at -80 ºC resulted in a decrease absorbance at 410 nm with a concomitant increase in absorbance at 548 nm, tentatively assigned to an Fe(III)-OOH species, with an isosbestic point maintained at 459 nm. The absorption band at 548 nm decays over 1000 s, however, in contrast to that observed at room temperature and at -30 ºC, the absorbance at 755 nm did not increase (Figure 17). Addition of 5 equiv. (Figure 18) or 10 equiv. (Figure 19) of H_2O_2 resulted in an increase in the rate of decrease in absorbance at 410 nm, again with a concomitant increase in absorbance at 548 nm.

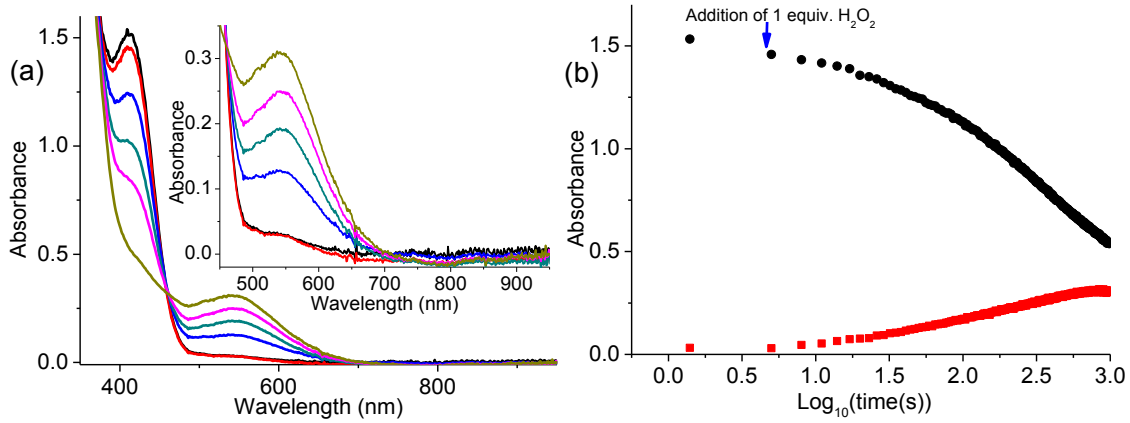

Figure 17 UV-vis absorption spectrum of **1** (1 mM) in acetone (black) at -80 ºC before, and (a) after addition of 1 equiv. H_2O_2, 3 s (red), 50 s (blue), 150 s (green), 300 s (pink), and 1000 s (olive green), and (b) time dependence of absorbance at 410 nm (red) and 543 nm (black).

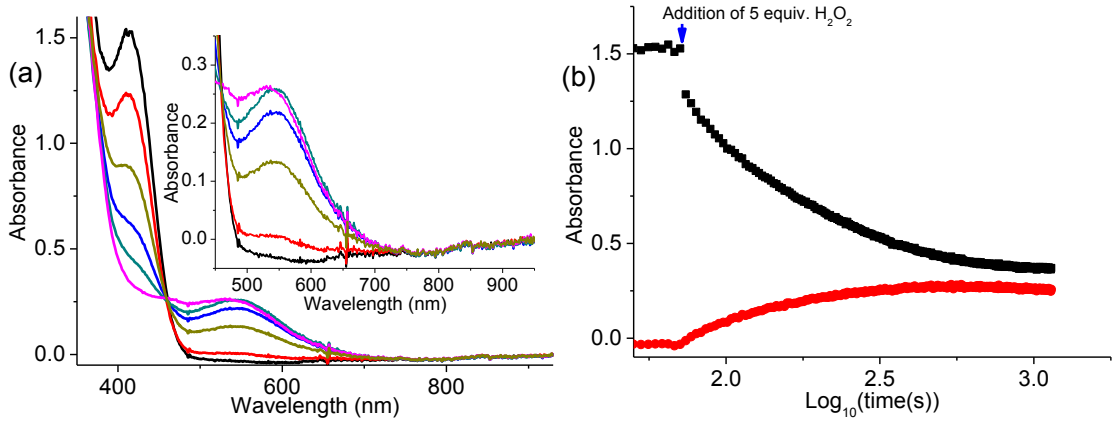

Figure 18 UV-vis absorption spectrum of 1 (1 mM) in acetone (black) at -80 ºC before and (a) after addition of 5 equiv. H_2O_2, 6 s (red), 70 s (grey), 150 s (blue), 300 s (green), and 1000 s (pink), and (b) time dependence of absorbance at 410 nm (black) and 543 nm (red).

Notably, with 10 equiv. H_2O_2 there is a subsequent shift in absorbance at 548 nm to 468 nm during the decay of the 548 nm absorbance indicative of formation of Fe(III)-OFe(III) acetato complexes (Figure 19). Again, there was no increase in absorbance at 755 nm. Addition of 25 equiv. H_2O_2 resulted in a yet more rapid decrease in absorbance at 410 nm and concomitant increase in absorbance at 548 nm, with an isosbestic point at 459 nm. The rate of the subsequent shift in absorbance maximum from 548 nm to 468 nm is also increased (Figure 20). Addition of 25 equiv. H_2O_2 (30 wt% instead of 50 wt%) to **1** in acetone (Figure 21a) or in acetone-d_6 (Figure 21c) resulted in a similar decrease in absorbance around 410 nm and concomitant increase in absorbance at 548 nm.

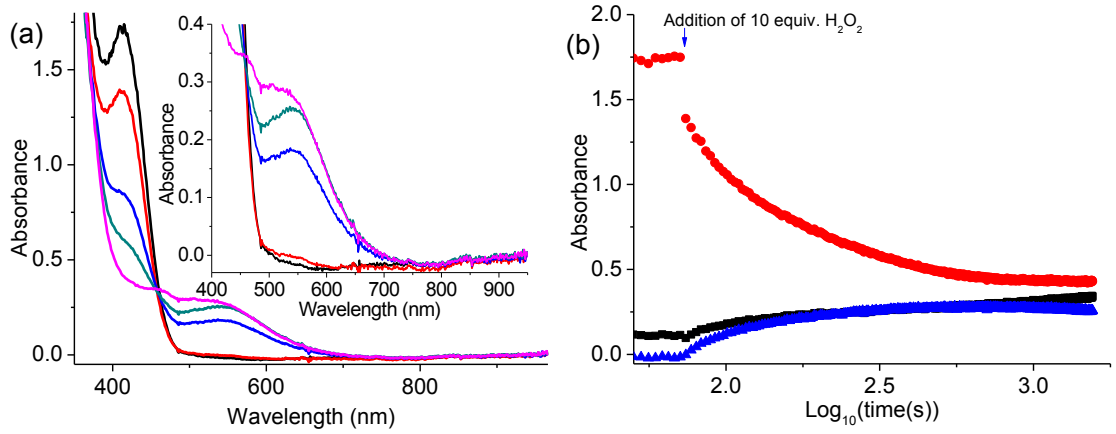

Figure 19 UV-vis absorption spectrum of 1 (1 mM) in acetone at -80 ºC (a) before (black) and after (a) 3 s (red), 70 s (blue), 200 s (green), and 1000 s (pink), and (b) time dependence of the absorbance at 410 nm (red), 473 nm (black) and 543 nm (blue).

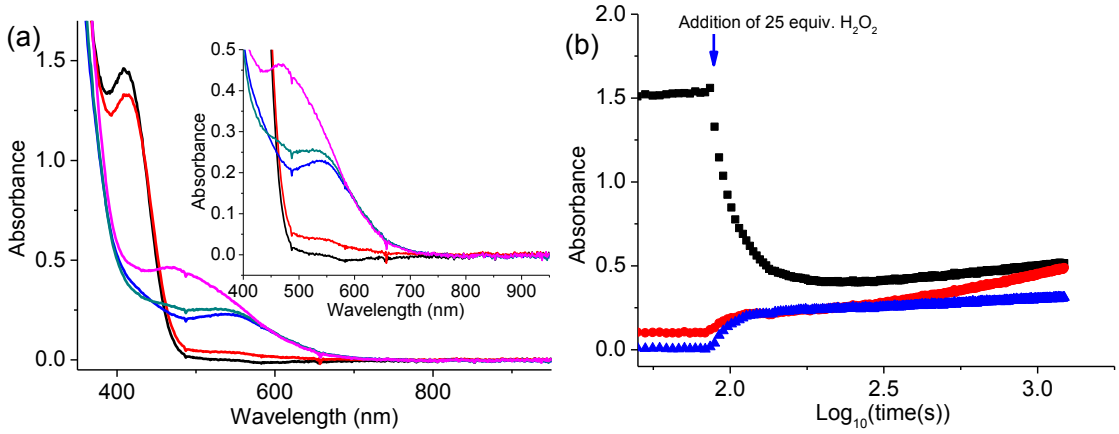

Figure 20 UV-vis absorption spectrum of 1 (1 mM) in acetone at -80ºC (a) before (black), and after addition of 25 equiv. H_2O_2, 6 s (red), 70 s (blue), 200 s (green), and 1000 s (pink), and (b) time dependence of absorbance at 410 nm (black), 473 nm (red) and 543 nm (blue).

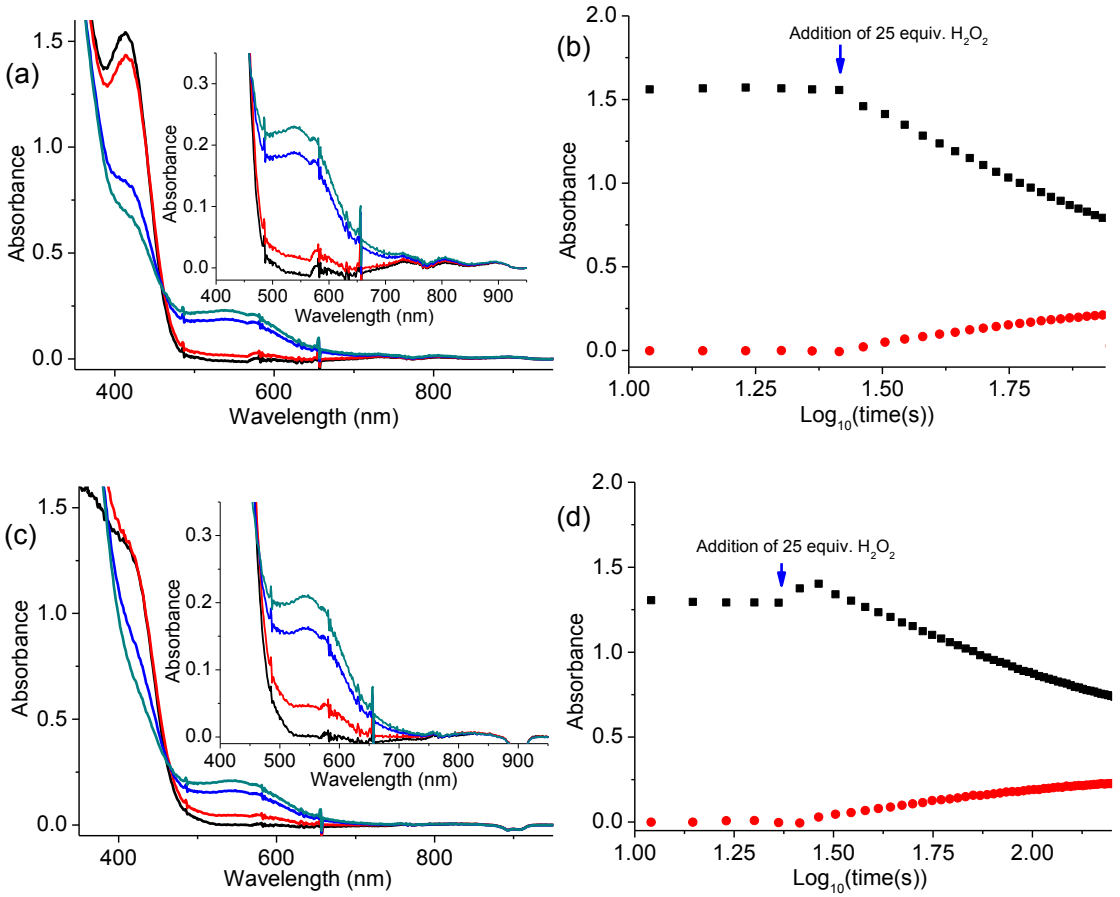

Figure 21 UV-vis absorption spectrum of 1 (1 mM) at -80 ºC (a) in acetone (black) before, and after addition of 25 equiv. H_2O_2 (30 wt%), 6 s (red), 50 s (blue), 78 s (green), (c) in D_6-acetone (black) before, and after addition of 25 equiv. H_2O_2 (30 wt%), 6 s (red), 50 s (blue), 100 s (green), (b) and (d) corresponding time dependence of absorbance at 410 nm (black), and 543 nm (red).

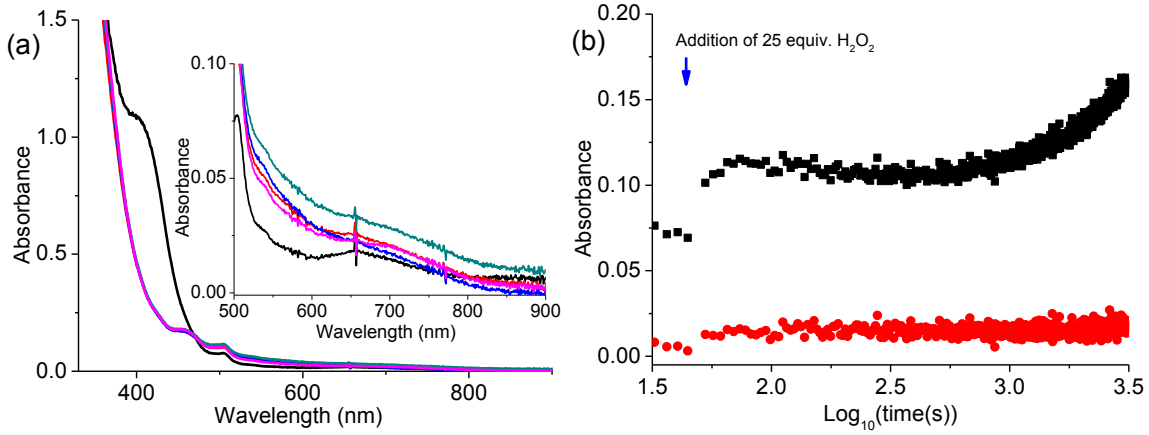

Figure 22 UV-vis absorption spectrum of **1** (1 mM) in (a) acetone with acetic acid (0.07 M, (black)) at -30 ºC before, and after addition of 25 equiv. H_2O_2,3 s (red), 50 s (blue), 100 s (green) and 500 s (pink), and (b) time dependence of absorbance at 503 nm (black) and 755 nm (red).

3.2.2 Reaction of 1 with H_2O_2 in acetone in presence of acetic acid

Addition of 25 equiv. H_2O_2 to **1** in acetone with excess acetic acid at -30 °C, resulted in a rapid decrease in Fe(II) absorbance, and immediate appearance of the characteristic absorption spectrum of an Fe(III)-O-Fe(III) acetato bridged dimer (Figure 22), with no evidence for formation of either the Fe(III)-OOH species (at 503 nm) nor the Fe(IV)=O species (at 755 nm). The effect of acetic acid on **1** in acetonitrile is studied in more detail in chapter 4.

3.2.3 Catalytic oxidation of alkenes at room temperature

Batchwise addition of 50 equiv. H_2O_2 (8.3 equiv. H_2O_2 at 5 min. intervals) to **1** in acetone was carried out for comparison with at the rate of addition of oxidant employed in earlier catalytic studies.[7] Addition of 8.3 equiv. H_2O_2 resulted in a rapid decrease in absorbance at 410 initially with a concomitant increase in absorbance at around 500 and 755 nm (Figure 23a) and ultimately formation of an Fe(III)-O-Fe(III) acetato complex.

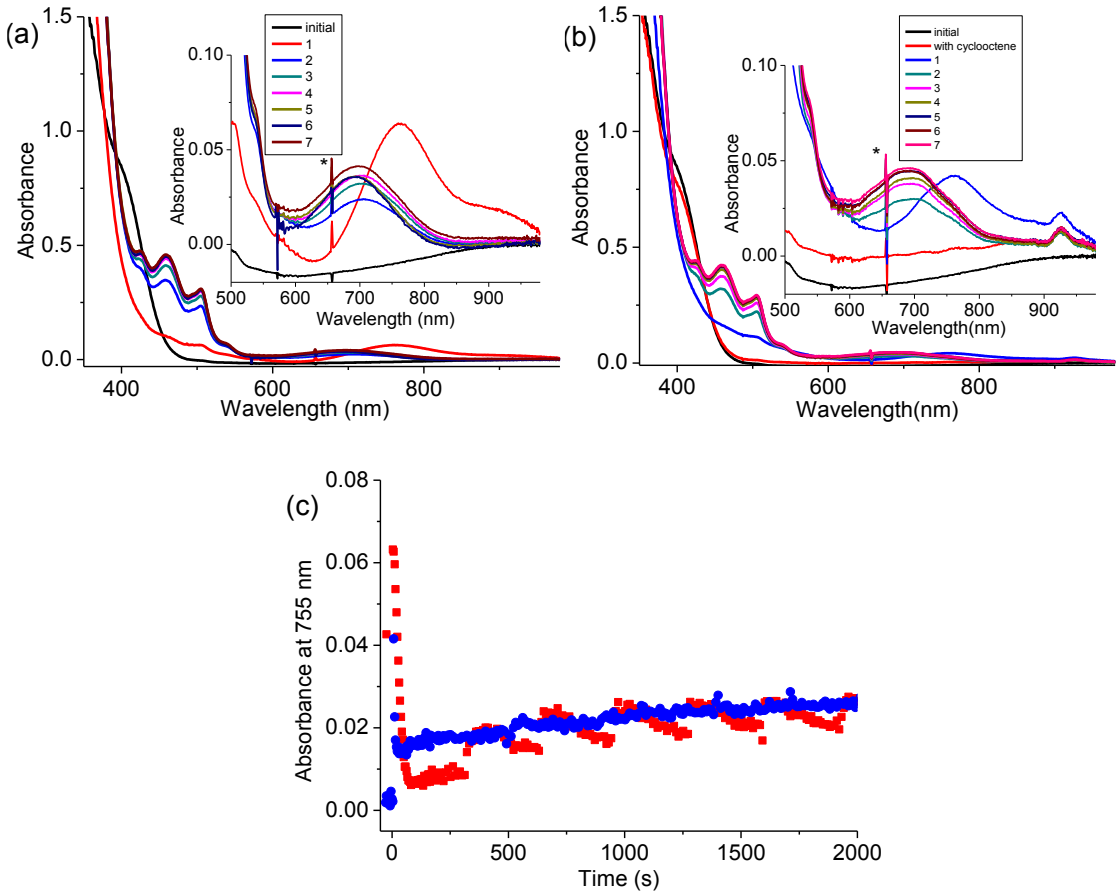

Figure 23 UV-vis absorption spectrum of **1** (1 mM) in acetone (black) at room temperature before, and (a) after batchwise addition of H_2O_2 over 30 min (8.3 equiv. every 5 min), (b) with *cis*-cyclooctene (0.88 M, 1000 equiv. (red)) and further addition of H_2O_2 over 30 min (8.3 equiv. every 5 min). (c) corresponding time dependence of absorbance at 755 nm without (red), and with *cis*-cyclooctene (blue).

Notably, the maximum extent of formation of the Fe(IV)=O species (at 755 nm) is substantially less after subsequent additions of H_2O_2 (Figure 23a). In presence of excess *cis*-cyclooctene the first addition of 8.3 equiv. of H_2O_2 resulted in the complete loss of the Fe(II) absorption (at 410 nm), however the maximum extent of increase of absorbance at 755 nm (Fe(IV)=O) is reduced and its decay is more rapid. Further additions of H_2O_2 does not result in the reappearance of the Fe(IV)=O absorbance, but instead only the characteristic absorption spectrum of the Fe(III)-O-Fe(III) acetato bridged complex was observed (Figure 23b).

In earlier studies the oxidation of *cis*-cyclooctene with H_2O_2 catalyzed by **1** in acetone was reported to yield the epoxide product as well as a mixture of cis- and trans-cyclooctane-1,2-diols.[7] The ^{1}H NMR spectrum of reaction mixture obtained after addition of H_2O_2 (six times 8.3 equiv. at 5 min intervals) to **1** with excess *cis*-cyclooctene, shows formation of cyclooctene epoxide (2.8 ppm), and a signal at 4.1 ppm (Figure 24a). The absence of signals from *trans*- nor *cis*-cyclooctane-1,2-diol, confirmed by spiking of the solution with independently prepared diols (Figure 24b), is notable and is not in agreement with analysis reported earlier by gas chromatography.[7]

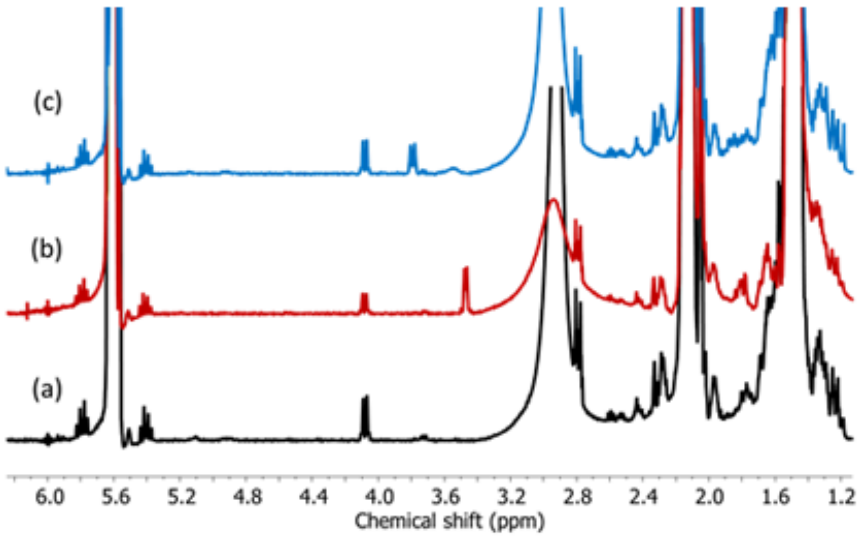

Figure 24 ^{1}H NMR (400 MHz) spectra of reaction mixture (a) obtained following batchwise addition of 50 equiv. H_2O_2 over 30 min to *cis*-cyclooctene (0.88 M, 1000 equiv.) and 1 (0.88 mM, 1 equiv.) in CD_3COCD_3 and spectra after addition of (b) *cis*-1,2-cyclooctane diol (69 equiv., 4.8 mg) to 0.55 ml, and (c) trans-1,2-cyclooctane diol (19 equiv., 1.2 mg) to 0.4 ml of the reaction mixture (a).

The stability of the cyclooctene epoxide formed during the reaction was confirmed by addition of 15 equiv. cyclooctene epoxide to the reaction mixture prior to addition of H_2O_2. The ^{1}H NMR spectrum of the reaction mixture after addition of H_2O_2 showed double the amount of epoxide and no significant change to the signal at 4.1 ppm (Figure 25).

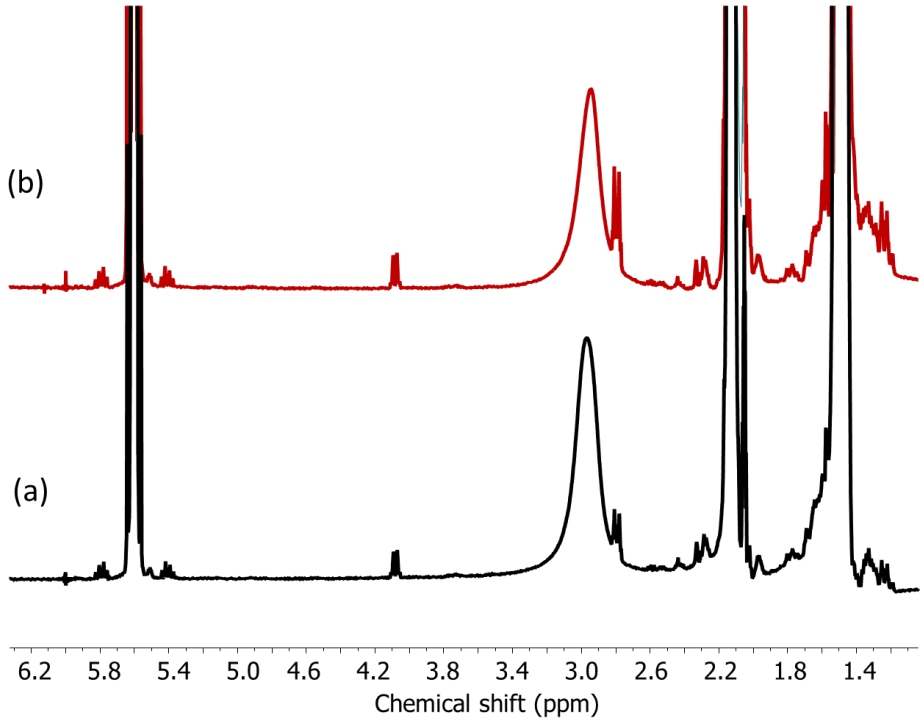

Figure 25 ^{1}H NMR (400 MHz) spectra of reaction mixture without (black) and with (red) addition of 15 equiv. of cycloctene oxide prior to addition of H_2O_2. See Figure 24 for further details.

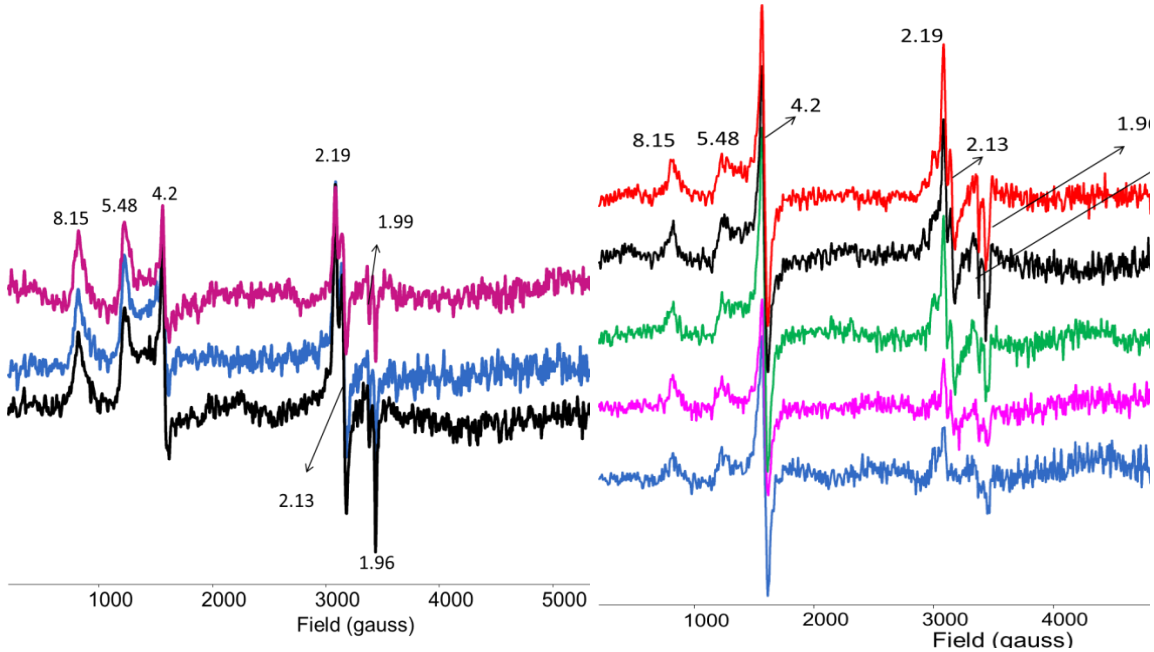

Figure 26 X-band EPR spectra (recorded at 77 K) after addition of 100 equiv. H_2O_2 to **1** (1 mM) in acetone (left) at -15 ºC, 5 s (black), 20 s (blue), and 180 s (pink), and (right) at -80 ºC, 5 s (blue), 20 s (pink), 160 s (green), 20 min (black), and 70 min (red)

3.2.4 EPR spectroscopy

X-band EPR spectra (recorded at 77 K) of aliquots flash frozen at the indicated times after addition of 100 equiv. H_2O_2 to **1** in acetone at -15 ºC (monitored by the UV-vis absorption spectroscopy), shows signals from both high and low spin Fe(III) complexes at g = 4.28, 5.48, 8.15, and g = 2.19, 2.13, 1.99 and 1.96, respectively. The intensity of the signals of the low spin Fe(III) complexes decreases over time, however, there was no significant change in intensity of signals due to high spin Fe(III) species (Figure 26, left). When the reaction was carried out at -80 ºC, the signals observed were similar, but in contrast to those obtained at -15 ºC, both the low spin and high spin signals increased in intensity over time (Figure 26, right). In the presence of acetic acid, the spectra obtained from the reaction at -80 ºC, shows signals at g = 4.28, 5.48, 8.15 from a high spin Fe(III) species and at g = 2.26 due to a low spin Fe(III) species (Figure 27). Notably, the signals at g = 2.19, 2.13,1.99 and 1.96 were not observed, consistent with UV-vis absorption data that indicated the absence of an Fe(III)-OOH species under these conditions.

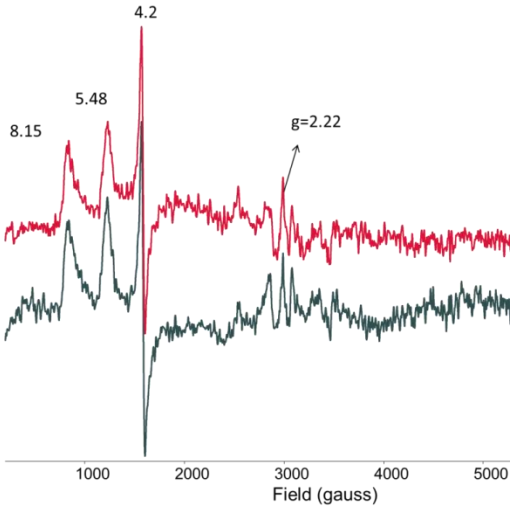

Figure 27 X-band EPR spectra (recorded at 77 K) of **1** (1 mM) in acetone with acetic acid (0.18 M) at - 80 °C, 5 s (black) and 4200 s (red) after addition of 100 equiv. H_2O_2.

3.2.5 ESI-MS spectroscopy

Cryospray ESI-mass spectra of **1** in acetone at -80 ºC shows m/z signals at $[LFe(II)OH_2]^{2+}$ - (182.0499) (L = MeN3Py), $[LFe(II)CH_3COCH_3]^{2+}$ - (202.0639), $[LFe(II)ClO_4]^{+}$ - (445.0437). Addition of 25 equiv. H_2O_2 to **1** at -80 ºC in acetone resulted in major m/z signals at $[LFe(IV)O]^{2+}$- (181.0398), $[LFe(III)CH_3CO_2]^{2+}$ - (202.5483), $[(LFe(III))_2(CH_3CO_3)]^{3+}$ - (255.7248), $[LFe(III)O_2]^{+}$ - (378.0731). Addition of 25 equiv. $H_2{}^{18}O_2$ showed major m/z signals at $[LFe(IV)O]^{2+}$ - (181.0398), $[(LFe(III))_2(CH_3C(^{18}O)(^{16}O)_2)]^{3+}$ - (256.3970), $[(LFe(III)CH_3C(^{18}O)(^{16}O)\ (ClO_4)]^{+}$ - (506.05569). In acetone-D_6 m/z signals were observed at $[LFe(II)OH_2]^{2+}$ - (182.0499), $[LFe(II)CD_3COCD_3]^{2+}$ - (205.0823), $[LFe(II)ClO_4]^{+}$ - (445.0437). Addition of 25 equiv. H_2O_2 to **1** at -80 °C resulted in m/z signals at $[(LFe(III))_2(CD_3CO_3)]^{3+}$ - (256.7337), confirming oxidation of acetone to acetic acid occurs under reaction conditions. The spectra obtained after addition of 25 equiv. H_2O_2 to **1** at -

80 ºC, -30 ºC or at room temperature in acetone were all similar (Table 1), indicating that the temperature within the mass spectrometer's ionization temperature dictated the species observed.

Table 1 Assignment of signals observed by cryospray ESI mass spectrometry at different temperatures.

m/z observed	species	charge
181.5456	[LFe(III)OH]	+2
231.0851	[LFe(II)(CH_3COCH_3)$_2$]	+2
236.6188	[LFe(II)(CD_3COCD_3)$_2$]	+2
405.1026	[LFe(III)CH_3CO_2]	+1
433.0597	[(LFe(III))$_2$(CH_3CO_3)]ClO_4	+2
434.0707	[(LFe(III))$_2$($CH_3C(^{18}O)(^{16}O)_2$]ClO_4	+2
434.5731	[(LFe(III))$_2$(CD_3CO_3)]ClO_4	+2
461.0251	[LFe(IV)(O)](ClO_4)	+1
504.0506	[LFe(III)(CH_3CO_2)]ClO_4	+1
965.0790	[(LFe(III))$_2$(CH_3CO_3)](ClO_4)$_2$	+1
965.0910	[(LFe(III))$_2$(CD_3CO_2)(O)](ClO_4)$_2$	+1

3.3 Discussion

The effect of solvent (acetone) in the reactions of **1** with H_2O_2 and the chemoselectivity observed in the oxidation of *cis*-cyclooctene oxidation was studied through a combination of UV-vis absorption, ^{1}H NMR, EPR, and ESI-mass spectroscopy techniques at ambient and low temperatures. A key step in the reaction of **1** with H_2O_2 is the exchange of the acetonitrile ligands with acetone which facilitates formation of the Fe(IV)=O species by enhancing the rate at which H_2O_2 reacts with **1**. A key challenge in the interpretation of the data obtained however is the *in situ* formation of acetic acid from acetone and the ultimate formation of a relatively stable Fe(III)-O-Fe(III) acetato bridged complex.

In acetone, the acetonitrile ligands of **1** exchange completely for acetone to form a high spin Fe(II) complex (Figure 1), with its corresponding paramagnetically shifted ^{1}H NMR spectrum and weak UV-vis absorption (^{5}MLCT) compared to **1** in acetonitrile.[12] These changes can be reversed by addition of acetonitrile. Cyclic voltammetry of **1** in acetone shows redox wave at 0.9 V, which is chemically irreversible and indicates that in the Fe(III) state co-ordination of adventitious water and formation of oxido bridged dinuclear complexes is preferred.[12]

In contrast to that observed in acetonitrile (see chapter 2), addition of stoichiometric amounts of H_2O_2, w.r.t **1**, at room temperature (20 °C) resulted in a complete loss of the visible absorbance of the Fe(II) complex and a rapid concomitant formation of a NIR absorbance ascribed to an Fe(IV)=O species. The λ_{max} (755 nm) of the Fe(IV)=O species

formed in acetone is at lower energy compared with that observed in acetonitrile (λ_{max} 725 nm, chapter 5), indicating a difference in the 6th ligand (acetonitrile vs acetone). The extent of increase in absorbance at 755 nm is increased with an increase in H_2O_2 (up to 5 equiv.) but decreases again with excess H_2O_2; indeed with > 25 equiv. H_2O_2 the absorbance at 755 nm was negligible. These data indicate that the Fe(IV)=O species can react with H_2O_2 to form an Fe(III) complex that subsequently undergoes ligand exchange to form an Fe(III)-OOH species (λ_{max} 503 nm, Scheme 1).

Ultimately the formation of an Fe(III)-O-Fe(III) acetato bridged complex occurs with its characteristic UV-vis absorbance spectrum and ESI mass spectral signals. Cyclic voltammetry shows 80% decrease in intensity of redox wave of **1** upon addition of 1 equiv. H_2O_2**,** and the appearance of a redox wave at 0.09 V, typical of Fe(III)-O-Fe(III) complexes (Figure 12). The oxidation of acetone to acetic acid was confirmed by ESI-mass spectrometry, with the shift of the signal due to $[(MeN3PyFe(III))_2(CH_3CO_2)(O)]^{3+}$ (m/z 255.7248) to $[(MeN3PyFe(III))_2(CD_3CO_2)(O)]^{3+}$ (m/z 256.7321) in acetone-D_6. Furthermore, it is clear that addition of acetic acid accelerates the formation of the Fe(III)-O-Fe(III) acetato bridged complex.

At -30 ºC, reaction of **1** with up to 5 equiv. H_2O_2 leads to formation of the Fe(IV)=O species, and the formation and decay is significantly slower compared to that observed at room temperature, however, again the species decay to an Fe(III)-O-Fe(III) acetato dimer. With 5 and 10 equiv. H_2O_2, the increase in the absorbance at 503 nm was observed, indicates formation an Fe(III)-OOH species, which decay to form the Fe(IV)=O species. The dependence on the number of equivalents of H_2O_2 indicates that the reaction of H_2O_2 with Fe(II), presumably via an Fe(II)-OOH species, leads to an Fe(IV)=O species through heterolytic O-O bond cleavage. Reaction of the Fe(IV)=O species with excess H_2O_2 leads ultimately to formation of the Fe(III)-OOH species (Scheme 2). In sharp contrast, at -80 ºC, addition of 1 equiv. H_2O_2 shows an increase in absorbance at 548 nm, tentatively assigned to Fe(III)-OOH species, which undergoes a shift to 503 nm with excess equiv. H_2O_2 (10 or 25 equiv.). EPR, which has high spin (g = 8.15, 5.48, 4.2) and low spin (g = 2.19, 2.13, 1.99, 1.96) indicating formation of an Fe(III)-OOH signals, and in contrast to the -15 °C, these signals increase over time. Notably, neither an Fe(IV)=O species nor an Fe(III)-O-Fe(III) acetato complex were observed at -80 ºC.

Although an earlier report[7] indicated that the oxidation of *cis*-cyclooctene with H_2O_2, catalyzed by **1** resulted in the formation of significant amounts of *trans*-cyclooctane-1,2-diol, in the present study the formation of neither *cis*- nor *trans*-cyclooctane-1,2-diol was observed by direct analysis of the reaction mixture by ^{1}H NMR spectroscopy, as confirmed by sample spiking. Indeed in the present study the formation of cyclooctene epoxide was confirmed together with the observation of a second product with a signal at 4.1 ppm, similar to hydoxy-cyclooctanone. The stability of cyclooctene oxide under the reaction conditions precludes that this latter product is the result of the former's

further oxidation. Hence, the product is most likely formed by oxidation of an initially formed *cis*- or *trans*-cyclooctane-1,2-diol; a process which appears to be highly efficient. Notably, from a mechanistic perspective, the presence of cyclooctene substantially diminishes the NIR absorbance of the Fe(IV)=O species formed indicating that it is this species that is responsible for substrate oxidation.

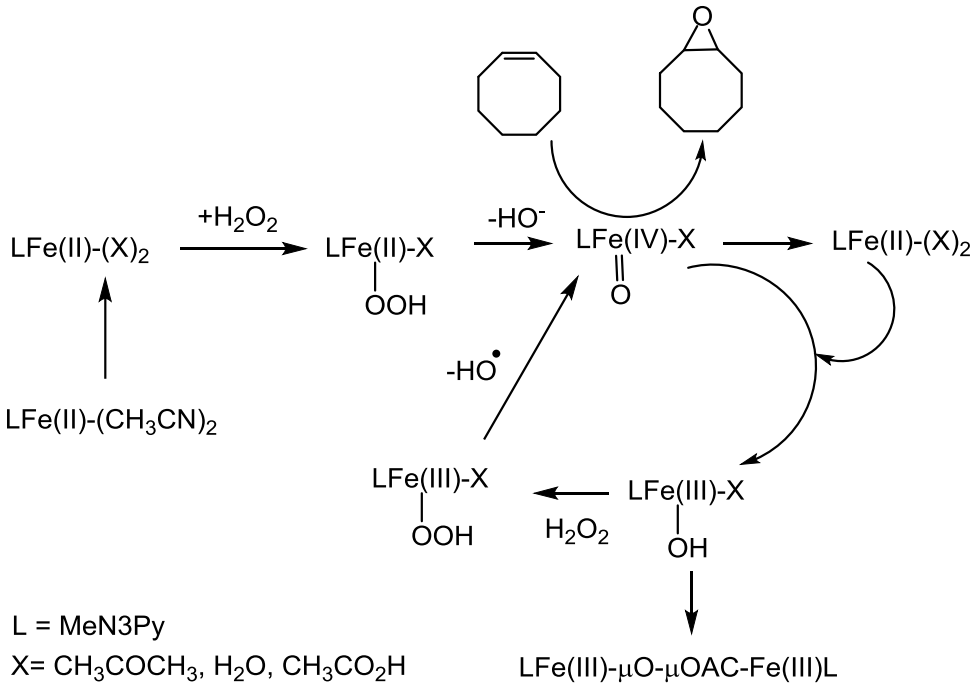

Scheme 2 General mechanism for the reaction of H_2O_2 with 1 in acetone, and *cis*-cyclooctene epoxidation.

3.4 Conclusions

In conclusion, the reaction of **1** with H_2O_2 in acetone at ambient and low temperatures and the reactivity of the various species formed with *cis*-cyclooctene indicate that an Fe(IV)=O species is responsible for substrate oxidation and that the exchange of the CH_3CN ligands of **1** with acetone facilitates rapid ligand exchange with H_2O_2 and hence formation of Fe(IV)=O at room temperature. The *in situ* formation of acetic acid leads to formation of a kinetically stable Fe(III)-O-Fe(III) acetato dimer, a process which is accelerated by addition of acetic acid. Moreover, stable formation of an Fe(III)-OOH species was observed at low temperatures (-30 and -80 °C), and absence of an Fe(IV)=O species at -80 °C indicates the barrier for the formation of this species (O-O bond homolysis) is relatively high.

A key finding under catalytic conditions is that the Fe(IV)=O species appears to react with the substrate to yield both diol and epoxide products but that the diols formed undergo subsequent oxidation to the correspondingly similar α-hydroxyketone product. Furthermore the shift in λ_{max} of the Fe(IV)=O species in acetone compared to acetonitrile indicates that they are distinct species presumably differing in the 6th ligand. Thus the

co-ordination site on iron center in acetonitrile, and acetone under reaction conditions plays a vital role in the chemoselectivity of the reaction. However, further studies are required to confirm if the formation of trans-diol reported previously does in fact take place.

3.5 Experimental section

See chapter 2 for experimental details.

Synthesis of *trans*-cyclooctane diol[15] Cyclooctene epoxide (710 mg, 5.6 mmol) was dissolved in acetonitrile (8.0 ml), to which TAHS (tetra butyl ammonium hydrogen sulfate, 769 mg, 2.2 mmol) dissolved in water (4.0 ml) was added with stirring, and refluxed for 2 days at 85 °C. Conversion was monitored by TLC. After 2 days, the reaction was cooled to room temperature and freshly prepared sat. $NaHCO_3$ (25 ml) was added. The reaction mixture was extracted with diethyl ether (3 x 10 ml). The separated organic layers were combined and dried over Na_2SO_4 and the solvent removed in vacuo. The crude product was purified by column chromatography (silica gel, pentane : diethyl ether (9:1), diethyl ether (10), ethyl acetate (10), methanol : ethyl acetate (0.2: 9.8)) to give an isolated yield 26% (200 mg). ^{1}H NMR (400 MHz, $CDCl_3$) δ 3.59 (dd, 2 H), 2.13 (s, broad, 2H), 1.86 (m, 2H), 1.6 (m, 10H) ppm.

3.6 References

1 Costas, M.; Mehn, M. P.; Jensen, M. P.; Que Jr, L. *Chem. Rev*. **2004**, *104*, 939-986.

2 Solomon, E. I.; Brunold, T. C.; Davis, M. I.; Kemsley, J. N.; Lee, S.-K.; Lehnert, N.; Neese, F.; Skulan, A. J.; Yang, Y.-S.; Zhou, J. *Chem. Rev*. **2000**, *100*, 235-350.

3 Girerd, J.-J.; Banse, F.; Simaan, A. J. *Struct. Bonding* **2000**, *97*, 143-177.

4 Parales, R. E. J. *J. Ind. Microbiol. Biotechnol.* **2003**, *30*, 271-278.

5 (a) Chen, K.; Costas, M.; Que, Jr., L. *J. Chem. Soc. Dalton Trans.* **2002**, 672-679. (b) Feng, J.; England, J.; Que, Jr., L. *ACS Catal*. **2011**, *1*, 1035-1042. (c) Suzuki, K.; Oldenburg, P. D.; Que, Jr., L. *Angew. Chem., Int. Ed.* **2008**, *47*, 1887–1889.

6 Roelfes, G.; Vrajmisu, V.; Chen, K.; Vrajmisu, K.; Ho, R. Y. N.; Rohde, J.-U.; Zondervan, C.; la Crois, R. M.; Schudde, E. P.; Lutz, M.; Spek, A. L.; Hage, R.; Feringa, B. L.; Munck, E.; Que Jr, L. *Inorg. Chem.* **2003**, *42*, 2639-2653.

7 Klopstra, M.; Roelfes, G.; Hage, R.; Kellogg, R. M.; Feringa, B. L. *Eur. J. Inorg. Chem.*, **2004**, 846-856.

8 Mas-Balleste, R.; Que, Jr, L. *J. Am. Chem. Soc.* **2007**, *129*, 15964-15972.

9 Makhlynets, O. V.; Oloo, W. N.; Moroz, Y. S.; Belaya, I. G.;Palluccio, T. D.; Filatov, A. S.; Muller, P.; Cranswick, M. A.; Que, L.,Jr.; Rybak-Akimova, E. V. *Chem. Commun.* **2014**, *50*, 645–648.

10 Payeras, A. M.; Ho, R. Y. N.; Fujita, M.; Que, Jr, L. *Chem. Eur. J.* **2004**, *10*, 4944-4953.

11 Oloo, W. N.; Meier, K. K.; Wang, Y.; Shaik, S.; Munck, E.; Que Jr, L. *Nat. Commun*. **2014**, *5*, 3046-3054.

12 Padamati, S. K.; Draksharapu, A.; Unjaroen, D.; Browne, W. R. *Inorg. Chem*. **2016**, *55*, 4211–4222.

13 Draksharapu, A.; Li, Q.; Logtenberg, H.; van den Berg, T. A.; Meetsma, A.; Killeen, J. S.; Feringa, B. L.; Hage, R.; Roelfes, G.; Browne, W. R. *Inorg. Chem.* **2012**, *51*, 900-913.

14 Lim, M. H.; Rohde, J.-U.; Stubna, A.; Bukowski, M. R.; Costas, M.; Ho, R. Y. N.; Munck, E.; Nam, W.; Que, L. Jr., *Proc. Natl. Acad. Sci. USA*, **2003**, *100*, 3665-3670.

15 Fan, R.-H.; Hou, X.-L. *Org. Biomol. Chem.* **2003**, *1*, 1565–1567.